

A&A manuscript no.
(will be inserted by hand later)

Your thesaurus codes are:
08 (02.01.2; 02.09.1; 08.02.3; 08.06.3; 08.14.1; 13.25.3; 13.25.5)

**ASTRONOMY
AND
ASTROPHYSICS**
December 2, 2024

High frequencies in the power spectrum of Cyg X-1 in the hard and soft spectral states.

M. Revnivtsev^{1,2}, M. Gilfanov^{2,1}, E. Churazov^{2,1}

¹ Space Research Institute, Russian Academy of Sciences, Profsoyuznaya 84/32, 117810 Moscow, Russia

² Max-Planck-Institute für Astrophysik, Karl-Schwarzschild-Str. 1, D-85740 Garching bei München, Germany,

Abstract. We analized a large number of RXTE/PCA observations of Cyg X-1 in the hard and soft spectral states with total exposure time of ≈ 190 and ≈ 10 ksec respectively and time resolution better than $\approx 250 \mu\text{s}$ in order to investigate its variability down to a few milliseconds time scales. The model of modifications of the power density spectra due to the dead time effect were tested using RXTE observations of an extremely bright source – Sco X-1. The results of these tests demonstrated that for sources like Cyg X-1 (which is an order of magnitude less bright than Sco X-1) present knowlegde of the instrument is fully sufficient to reliably analyze power density spectra up to high frequencies.

In both spectral states of Cyg X-1 we detected statistically significant variability up to ~ 150 – 300 Hz with a fractional rms amplitude above 100 Hz at the level of ~ 2 – 3% . The power spectrum in the hard state shows a steepening at frequency of ~ 40 – 80 Hz with the power law slope changing from ~ 1.7 to ~ 2.3 – 2.4 . In the soft state the slope of power spectrum changes from ~ 1 to ~ 2 at the frequency of ~ 15 – 20 Hz without any evidence of further steepening up to ~ 100 – 150 Hz. These break frequencies represent the highest characteristic frequencies detected in the power density spectrum of Cyg X-1 so far.

Key words: Accretion, accretion disks – Instabilities – Stars:binaries:general – Stars:classification – Stars:neutron X-rays: general – X-rays: stars

1. Introduction

The shortest timescales in the variability of the compact objects always was very interesting topic of X-ray astronomy. The efforts to measure the highest frequency in the variabilty of Cyg X-1 can be traced back to

rocket experiments in 70-ties (e.g. Rothschild et al. 1974, Giles 1981). It was found that Cyg X-1 demonstrates statistically significant variability of the X-ray flux at least up to frequencies of ~ 10 Hz. Since then Cyg X-1 was extensively observed by various satellite missions searching for millisecond and submillisecond time scales variability (HEAO-1, see e.g. Meekins et al. 1984, Wen et al. 1996; EXOSAT, e.g. Belloni & Hasinger 1990; GINGA, e.g. Miyamoto & Kitamoto 1989). At the present time the Rossi X-ray Timing Explorer observatory (RXTE, Bradt, Rothschild & Swank 1993) is the most powerful experiment for the investigation of the short time scale X-ray flux variations. It combines high telemetry rate (up to 512 kbps), high effective area of the detectors ($\sim 6400 \text{ cm}^2$ in the soft X-ray band), high time resolution (down to $1\mu\text{sec}$) and comparatively low deadtime distortions. The comparison of the characteristics of several X-ray experiments can be found in e.g. Giles, Jahoda & Strohmayer 1998.

The shape of the power density spectrum (PDS) of Cyg X-1 in its low/hard spectral state is well established (in the range from $\sim 10^{-3}$ to ~ 50 – 100 Hz) since EXOSAT observations – it can be roughly represeted by a constant from $\sim 10^{-3}$ Hz up to some break frequency ($P \sim f^0$), than it steepens to the power law with index ~ -1 ($P \sim f^{-1}$) and then it breaks again to the power law with the index ~ -1.6 – -1.8 , $P \sim f^{-1.6-1.8}$ (see e.g. RXTE results in Nowak et al. 1999). Short observations (~ 10 ksec) of Cyg X-1 by RXTE/PCA with high time resolution ($\sim 4\mu\text{s}$) showed the absence of significant variability of Cyg X-1 at time scales smaller than ~ 3 msec (Giles, Jahoda & Strohmayer 1998).

In this paper we report the systematic study of very high frequency variability of Cyg X-1 in X-rays using large number of RXTE observations (total exposure time close to 190 ksec for the hard state and ~ 10 ksec for the soft state) and carefully treating the deadtime effects.

2. Observations, data reduction and deadtime corrections

For our analysis we used the data from the Proportional Counter Array (PCA) aboard RXTE. To study the source variability in the hard spectral state, we chose a compact group of observations of Cyg X-1 performed on 15–17 Dec. 1996 (proposal P10236) with total exposure time of ~ 80 ksec and 56 available observations of Cyg X-1 from the proposal P30157 performed between Dec. 1997 and Dec. 1998 with total exposure time of ≈ 110 ksec. The soft spectral state data were accumulated on 4–18 June 1996 data (proposal P10512, see also Cui et al. 1997) with total exposure time of ≈ 10 ksec. All observations were performed with 5 PCUs switched on.

The power density spectra were calculated from the light curves with the bin duration equal to the intrinsic time resolution of the data ($2^{-13}s \approx 122\mu s$ in proposals P10236 and P10512 and $2^{-12}s \approx 244\mu s$ in proposal P30157). Some deviations from the noise level predicted by the PCA dead time models are observed in the power spectra constructed in the PCA energy sub-bands with the amplitude of $\sim 10^{-6}$ (rms/mean) 2 /Hz. We therefore followed recommendations of the RXTE GOF and analyzed the light curves in the total PCA energy band, where these deviations seem to be considerably less significant (William Zhang, private communication).

The power spectra calculated for individual time series were normalized to units of squared fractional rms

$$P_j = \left(\frac{2|a_j|^2}{N_\gamma} - 2 \right) \frac{1}{R_{\text{tot}}}$$

and averaged. In the above formula a_j is the Fourier amplitude at the frequency f_j ; N_γ – is total observed number of counts in the time series; R_{tot} – averaged observed count rate for the time series. Note that the ideal Poissonian noise component is already subtracted, therefore $P_j = 0$ for a Poissonian distribution of counts in the time series.

In a real detector various effects could lead to modification of the Poissonian noise level by an amount ΔP . Two major effects contribute to ΔP in the case of PCA detector:

$$\Delta P = \Delta P_{\text{dt}} + \Delta P_{\text{vle}}$$

where ΔP_{dt} is a modification of the noise level due to counts dead time, ΔP_{vle} – additional noise component resulting from vetoing of the PCA detectors by the Very Large Events (VLE).

With an accuracy sufficient for our purpose the PCA dead time caused by the incident photons can be described as a non-paralizable process ¹ (Jahoda et al. 1996),

¹ However, there is small paralizable component in the total instrument deadtime (Jahoda et al. 1996). The value of paral-

for which modification of the noise level was derived by Vikhlinin, Churazov & Gilfanov 1994 (see also Zhang et al. 1995 for the expression accounting for finite length of the time series). We shall use below the equation (A4) from Vikhlinin, Churazov & Gilfanov 1994 transformed to the units of squared fractional rms:

$$\Delta P_{\text{dt}}(\tau_d, t_b, R) = -4 \cdot \frac{1}{R} \cdot \sin(2\pi f t_b/2)^2 \times \sum_{k=-k_m}^{k_m} X[2\pi(f + k/t_b)]/(\pi(f t_b + k))^2 \quad (1)$$

where

$$X[f] = \frac{R'^2[1 - \cos(2\pi f \tau_d)] + R' 2\pi f \sin(2\pi f \tau_d)}{R'^2[1 - \cos(2\pi f \tau_d)]^2 + [R' \sin(2\pi f \tau_d) + 2\pi f]^2};$$

$$R' = \frac{R}{1 - R \tau_d}$$

Here R is the observed count rate, τ_d is the photon dead time, t_b is the bin duration, f is the frequency. For the practical purposes k_m of the order 10 is sufficient. This equation (for $k_m = \infty$) is valid for an infinitely long time sequence. One can use more complicated expression (see equation (44) from Zhang et al. 1995) if the analyzed time sequence contains only small number of bins.

To the first approximation the Very Large Events lead to appearance of an additional (positive) component (Zhang et al. 1996)

$$\Delta P_{\text{vle}}(f, \tau_{\text{vle}}, R_{\text{vle}}) = 2R_{\text{vle}}\tau_{\text{vle}}^2 \left[\frac{\sin(\pi\tau_{\text{vle}}f)}{\pi\tau_{\text{vle}}f} \right]^2 \quad (2)$$

where τ_{vle} – the duration of the VLE window, R_{vle} – the VLE count rate in one PCU. Note that the above expression does not include the binning and sampling effects and is valid in the limit $R_{\text{vle}}\tau_{\text{vle}} \ll 1$.

Finally, the total noise component model in the first approximation would be:

$$\Delta P = \frac{1}{N_{\text{pcu}}} [\Delta P_{\text{dt}}(\tau_d, t_b, R_{\text{pcu}}\mu_{\text{vle}}) \mu_{\text{vle}} + \Delta P_{\text{vle}}(\tau_{\text{vle}}, R_{\text{vle}})]$$

$$\mu_{\text{vle}} = \frac{1}{1 - R_{\text{vle}}\tau_{\text{vle}}}$$

where R_{pcu} – the total observed count rate in one PCU, N_{pcu} – number of PCUs. The $\Delta P_{\text{dt}}(\tau_d, t_b, R)$ and $\Delta P_{\text{vle}}(\tau_{\text{vle}}, R_{\text{vle}})$ are given by the equations (1) and (2) respectively. The factor $1/N_{\text{pcu}}$ accounts for the fact that the count streams from N_{pcu} independent units were merged together. The factor μ_{vle} accounts for reduction of the observed count rate due to Very Large Events. This formula

izable deadtime in principle can slightly depend on the hardness of the source

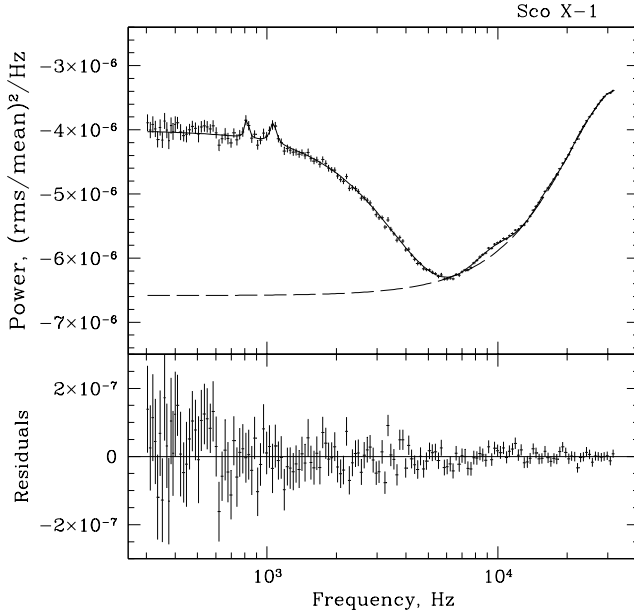


Fig. 1. The power spectrum of Sco X-1 from the observation #1 performed with medium VLE window. The solid line shows the best fit model consisting of the noise level model ΔP and two kHz QPOs (see text). The dashed line shows the noise level component ΔP_{dt} due to photon dead time. The lower panel shows the residuals data–model.

is valid under the following conditions: $R_{\text{vle}} \ll R_{\text{pcu}}$, $R_{\text{vle}}\tau_{\text{vle}} \ll 1$ and $\tau_{\text{vle}} \gg \tau_{\text{dt}} R_{\text{pcu}} (\tau_{\text{dt}} + 1/R_{\text{pcu}})$. It is important to stress out that in the adopted dead time model R_{pcu} is the the *total observed* count rate of the events causing the dead time τ_d (as opposite to the observed count rate in the analyzed time series). In the case of PCA detector it should include total Good Xenon rate, Propane and Remaining counts. We also note that for sufficiently small count rates, $R \lesssim 3\text{--}5$ kcnts/sec/PCU dependence of ΔP_{dt} (τ_d, t_b, R) and, therefore, of ΔP upon R vanishes. The model has been tested on a series of Monte-Carlo simulations and has proven to be sufficiently accurate in the parameters range of interest.

Note that we did not include in our model an additional background term (Jahoda 1998 or Jernigan, Klein & Arons 2000). For bright sources ($\gtrsim 1$ kcnts/sec/PCA) its contribution can be neglected.

To verify our model for the noise component we compared it with the data of PCA observations of an extremely bright source Sco X-1 ($\sim 100\,000$ cnts/s/PCA) for which all flavors of the dead time distortions are much more prominent than for Cygnus X-1. We used 3 different observations of Sco X-1 – 10059-01-01-00 (Feb. 14, 1996; hereafter #1), 10059-01-03-00 (Feb. 19, 1996; #2) and 10056-01-02-02 (May 26, 1996; #3), having different value

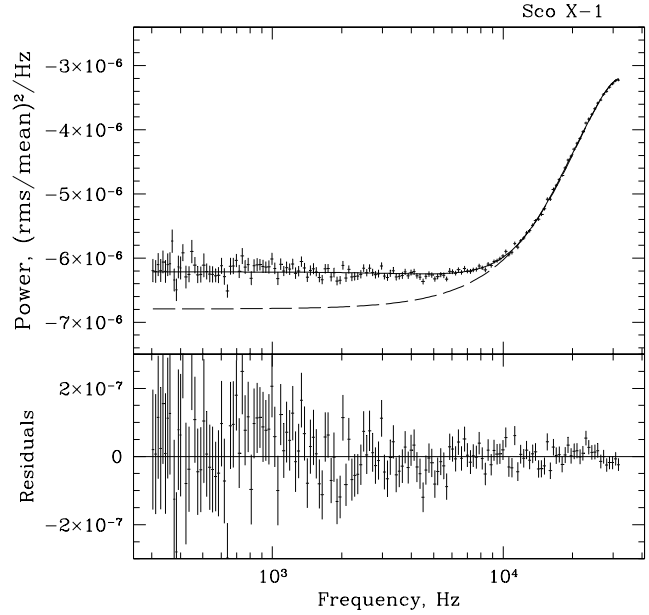


Fig. 2. The same as Fig.1 but for observation #2, performed with short VLE window.

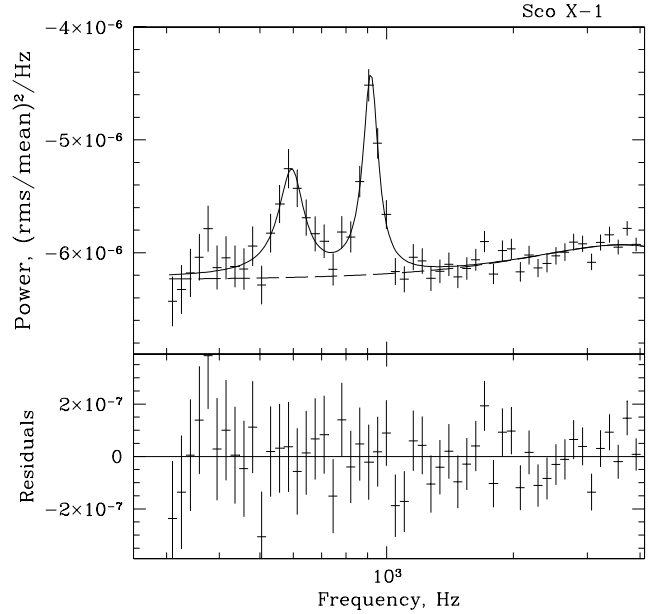


Fig. 3. The same as Fig.1 but for observation #3, performed with short VLE window and lower time resolution, $\approx 122\ \mu\text{s}$.

of the VLE window τ_{vle} and different time resolution. Ideally, once the values of the dead time τ_d and VLE window τ_{vle} are calibrated, the model should reproduce the noise level with count rates R_{pcu} and R_{vle} set to the measured values. However, as we discuss below, this is not strictly

Table 1. The expected and best fit model parameters of the deadtime correction for 3 observations of Sco X-1.

Obs.ID.	$t_b, \mu s$	$t_d, \mu s$		$R_{pcu}, \text{kcnts/s}$				$\tau_{vle}, \mu s$		$R_{vle}, \text{cnts/s}$	χ^2/dof
		exp.	fit	Tot ^b	GX^c	fit	exp. ^d	fit	exp. ^e	fit	
#1	15.25879	8–10 ^a	8.5 ± 0.1	29.2	20.8	17.6 ± 0.3	150	152 ± 1	265	274 ± 2	152/151
#2	15.25879	8–10 ^a	8.7 ± 0.1	19.6	15.1	10.0 ± 0.5	60	76 ± 2	239	244 ± 13	180/157
#3	122.0703	8–10 ^a	8.7(fixed)	23.6	18.3	14(fixed)	76.0(fixed)	157	162 ± 6	43/46	

^a – e.g. Jahoda et al. 1996, Jahoda et al. 1997

^b – measured total count rate (Good Xenon, Propane Counts and Remaining Counts) per PCU

^c – measured Good Xenon count rate per PCU

^d – preflight values for all PCA, see Giles 1995

^e – measured count rate (HouseKeeping data)

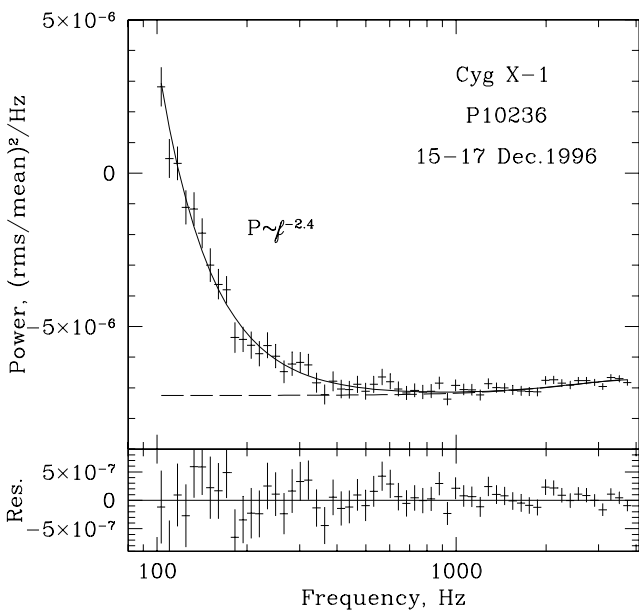


Fig. 4. The power spectrum of Cyg X-1 (observations 15–17 Dec., 1996; proposal P10236). Total exposure time $\sim 80\text{ksec}$. Dashed line shows the instrumental noise level.

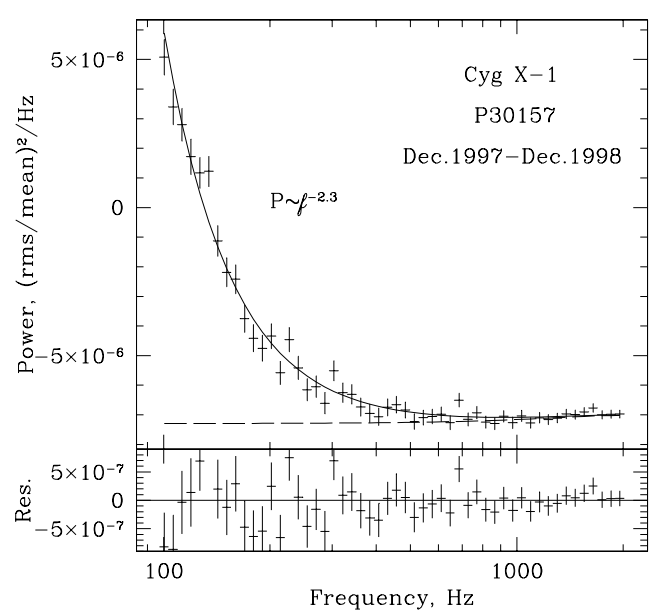


Fig. 5. The same as Fig. 4 but for observations from proposal P30157 (Dec. 1997–Dec. 1998, hard spectral state). Total exposure $\sim 110\text{ksec}$.

the case. We therefore followed the approach adopted by Jernigan, Klein & Arons 2000 and fitted the power spectra at high frequencies, $f > 300\text{ Hz}$, with the model for the noise component plus the model for the source component leaving the noise model parameters free. The source contribution in this particular case was modeled as a superposition of two Lorentzians representing kHz QPOs. This approach has a disadvantage that it requires a priori assumptions about the shape of the power spectrum of the source. In particular, if the source has very weak and very flat power spectrum component it might be not detected by our procedure.

In Fig. 1, 2 and 3 we present the power spectra of Sco X-1 in observations #1 #2 and #3 along with the best fit noise models and residuals. The best fit parameters and their expected values are given in Table 1. For observation #3 we fixed parameters t_d , R_{pcu} and τ_{vle} because the limited frequency range of the power spectrum ($<4096\text{ Hz}$) does not allow us to constrain their values from the fit. From Fig. 1, 2 and 3 one can see that with appropriate tuning of the parameters the adopted noise model is capable to reproduce the observed shape of the noise component.

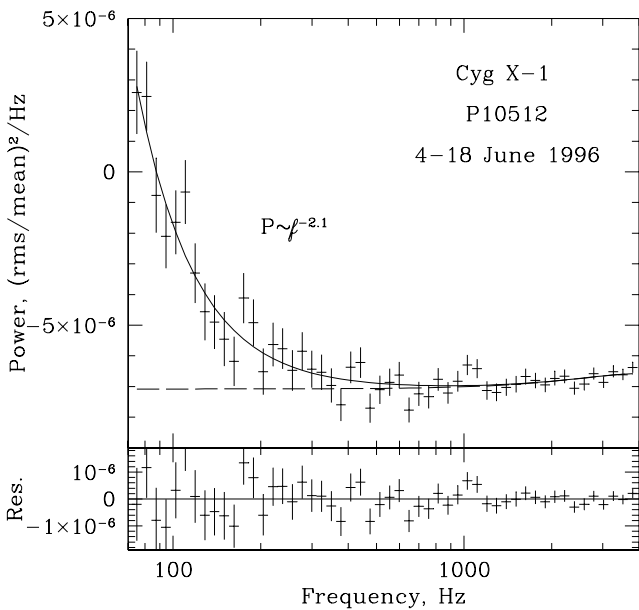


Fig. 6. The same as Fig. 4 but for observations from proposal P10512 (4-18 June, 1996, soft spectral state). Exposure ~ 10 ksec.

In general the best fit parameters of the noise level model (Table 1) look reasonable and are close to the expected values. The best fit value of τ_{vle} , in observation #2 is by $\approx 30\%$ higher than the preflight value. It is possible, however, that the duration of the VLE window differs from the preflight values (Alan Smale, private communication). The most apparent difference is a large, by a factor of ~ 2 , discrepancy between the best fit and observed total count rate. But we should note that the observed GoodXenon count rate is much closer to the best fit R_{pcu} value (see Table 1). The reason of this discrepancy is not clear, it might be due to unaccounted processes in the PCA detectors at high count rates. We note however, that dependence of the noise component (in units of squared fractional rms) on the total count rate is a specific feature of a non-paralyzable dead time process at sufficiently high count rates. At lower count rate ($R_{\text{pcu}} \lesssim 3000-5000$ cnts/s) and in particular in the case of Cyg X-1 ($R_{\text{pcu}} \sim 1000-1500$ cnts/s) this dependence vanishes.

3. Results

We adopted the noise level model described in the previous section for the subsequent analysis of the Cyg X-1 data. Since the Cyg X-1 observations were performed with time resolution coarser than $\approx 122 \mu\text{sec}$, the photon dead time and duration of the VLE window are not constrained by

the data. We fixed them at the best fit values determined from the Sco X-1 data: $t_d = 8.7 \mu\text{s}$ and $\tau_{\text{vle}} = 76 \mu\text{s}$. As mentioned above, at the count rates typical for Cyg X-1, $R_{\text{pcu}} \sim 1000-1500$ cnts/s, the noise level does not depend on the count rate. We therefore fixed the R_{pcu} parameter at the averaged observed value. The only free parameter of the noise level model was R_{vle} . Similarly to the procedure applied to the Sco X-1 data, we included the source component into the model. The source component was represented by a power law $P \propto f^{-\alpha}$. We used the high frequency part of the power spectra, from 100 Hz up to the Nyquist frequency, for the fits.

The high frequency part of the observed power spectra of Cyg X-1 before subtraction of the noise level $\Delta P(f)$, the best fit model and the residuals of the data from the model are shown in Fig. 4, 5 and 6. The overall power spectra in a broad frequency range from 1 mHz to ≈ 2 kHz after subtraction of the best fit noise level model are shown in Fig. 7. One can see that the model describes the data points reasonably well: $\chi^2 \sim 38/55$ dof for observations P10236 (Fig. 4), $\chi^2 \sim 56/49$ dof for observations P30157 (Fig. 5) and $\chi^2 \sim 46/49$ for observations P10512 (soft state, Fig. 6). The best fit values of the slope of the source power spectrum are: $\alpha = 2.4 \pm 0.1$ for P10236, $\alpha = 2.27 \pm 0.08$ for P30157 and $\alpha = 2.1 \pm 0.2$ for P10512. The intrinsic variability of the source has been statistically significantly detected up to frequencies of $\sim 150-300$ Hz (Fig. 4-6) with the fractional rms amplitude in frequency band $\sim 100-400$ Hz of $\approx 3\%$ (hard spectral state) and $\approx 2\%$ (soft state).

In order to increase statistics we averaged all the hard state data increasing the total exposure time up to ≈ 190 ksec. The power law approximation of the averaged power spectrum above 100 Hz gives the power law index of $\alpha = 2.32 \pm 0.07$. The power law approximation of the same data in the 20-60 Hz frequency range results in $\alpha = 1.66 \pm 0.01$, although the PDS clearly has a more complicated shape than a power law (Fig. 8). We therefore conclude that we detected statistically significant steepening of the power spectrum of Cyg X-1 in the hard state at the frequency of $\sim 40-80$ Hz. Note, that some indication of such steepening can be found in Nowak et al. 1999, although short duration of the used observations (~ 20 ksec) was not sufficient to study the high frequencies in detail. In order to illustrate the high frequency behaviour of the power spectra, we plot in Fig. 8 the power spectra multiplied by f^2 . As it can be seen from Fig. 8 the particular shape of the rollover above 100 Hz is not significantly constrained by the data. Assuming that power spectrum continues with the same slope to the higher frequencies an observatory of the EXTE/LASTE class (effective area $\sim 10 \text{ m}^2$, Barret 2000) would be able to detect statisti-

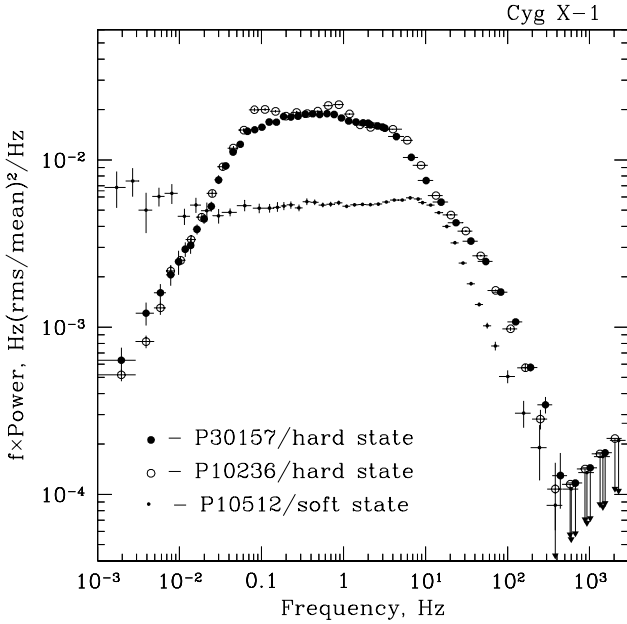


Fig. 7. The broad band (10^{-3} – 10^3 Hz) power spectrum of Cyg X-1 in the hard and soft spectral states state averaged over different data sets used for the analysis. The power spectra were multiplied by the frequency.

cially significant signal up to several kHz in \sim tens of ksec exposure time and help us to say something more about the exact shape of the rollover of the PDS.

The 2σ upper limit on the amplitude of a possible QPO component (Lorentz profile with quality Q) in the 500–2000 Hz frequency range in the hard state power spectrum is $\sim 2\%$ for $Q = 1$ and $\sim 0.9\%$ for $Q = 20$. These upper limits were obtained using the observations from the proposal P10236 performed on 15–17 Dec. 1996 in which the shape of the power density at the lower frequency did not vary significantly. The upper limit on the continuum noise component at the high frequency is somewhat more difficult to estimate. A statistical (2σ) error on the fractional rms in the 500–2000 Hz for the sum of all hard state observations is $\approx 1\%$. Assuming that the noise level model is exact the upper limit on the fractional rms would coincide with the above number. However, as we mentioned in the previous section a weak and very flat source power spectrum component might be not detected given the procedure used to determine the instrumental noise level.

4. Summary

We analyzed ~ 190 ksec of observations of Cyg X-1 in the low/hard state and reanalyzed ~ 10 ksec of high/soft state observations. We detected statistically significant variability up to frequencies of ~ 300 – 400 Hz with the fractional

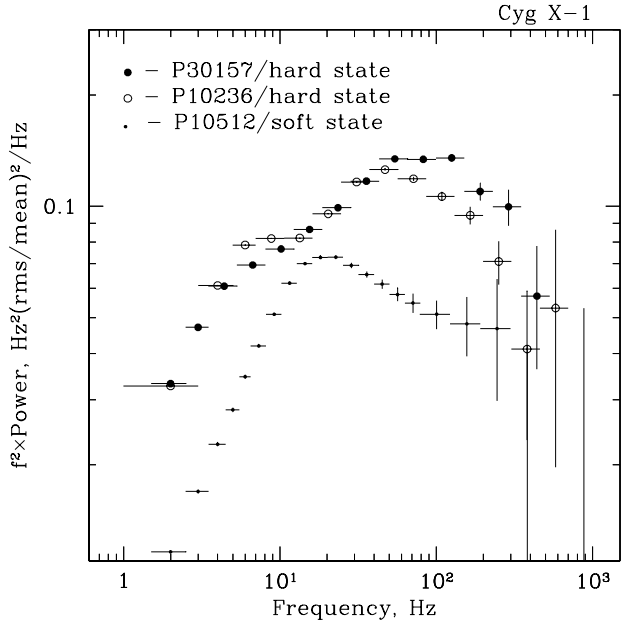


Fig. 8. The power density spectrum of Cyg X-1 at high frequencies. Note, that the power spectrum has been multiplied by f^2 .

rms amplitude in the 100–400 Hz frequency range $\approx 3\%$ in the hard state and $\approx 2\%$ in the soft state. The 2σ upper limits on the fractional rms amplitude of a QPO feature with Lorentzian profile in the 500–2000 Hz frequency range are $\sim 2\%$ for $Q \sim 1$ and $\sim 0.9\%$ for $Q \sim 20$ in the hard state and 2.5% ($Q \sim 1$) and 1.5% ($Q \sim 20$) in the soft state. Assuming that the model for the instrumental noise level is exact, the 2σ upper limits on the continuum variability in the 400–2000 Hz frequency range are $\sim 1\%$ and $\sim 1.7\%$ for the hard and soft state respectively.

We detected statistically significant steepening of the power spectrum in the hard state at frequencies ~ 40 – 80 Hz. The power law approximation to the spectrum at frequencies higher than ~ 80 – 100 Hz gives the slope of $\alpha \sim 2.3$ – 2.4 . In the soft state the slope of power spectrum changes from ~ 1 to ~ 2 at the frequency of ~ 15 – 20 Hz without any evidence of further steepening up to the frequency of ~ 100 – 150 Hz.

Thus the sensitivity and time resolution of the RXTE allow one to probe interesting range of the variability time scales for accreting black holes. Several characteristic frequencies fall approximately in this range. First of all the frequency of rotation at the last marginally stable orbit for the non-rotating (Schwarzschild) black hole is $f \sim 200 \frac{10M_\odot}{M}$ Hz. For the maximally rotating Kerr black hole this frequency ranges from ~ 1200 Hz to ~ 150 Hz for the co-rotating and counter-rotating orbits respectively.

If Keplerian rotation itself makes significant contribution to the variability of the X-ray flux (e.g. due to the Doppler shift and boosting of the emission from the “hot spots” in the disk) this difference should be manifested in this frequency range (Sunyaev 1972). Secondly typical sound crossing time of the disk height (in the case of optically thick geometrically thin standard accretion disk) corresponds to the frequency of hundreds of Hz. If strong turbulence is present in the accretion flow as anticipated by the most popular theoretical models (see e.g. Balbus & Papaloizou 1999 for review) then it may affect the variability at higher frequencies. The dependence of the amplitude of variations on the frequency is then a valuable tool to study the turbulence in the accretion flow. Thirdly light crossing time of the central region $t_{lc} = 3R_g/c \sim$ corresponds to the frequencies of the order of kHz. The light crossing time for the region of the main energy release ($R \sim 10-20 R_g$) corresponds to the frequencies of 300–500 Hz. The character of the the variability may change drastically around this frequency or (e.g. in the componization models involving multiple scatterings of the photons) at a several times lower frequencies (e.g. Payne 1980, Sunyaev & Titarchuk 1980, Pozdnyakov, Sobol & Sunyaev 1983, Nowak & Vaughan 1996).

The RXTE data (i) demonstrate that power specifically associated with any of these characteristic frequencies is not large (see given above upper limits on the narrow features on the PDS in the frequency range from 500–2000 Hz) – i.e. there are no “resonances” at these frequencies, (ii) limits the total power associated with high frequency variability (from 400 Hz to 2000 Hz) to a percent level, (iii) show that in the hard state of the source prominent, previously unknown, break in the PDS occurs at the frequency of ~ 70 Hz, (iv) extend the range of significantly detected variations up to the frequencies of $\sim 200-300$ Hz. The theoretical models of the accretion onto the black holes are now to be tested against these results. The study of the high frequency noise might become an additional tool to distinguish black holes from weakly magnetized neutron stars (Sunyaev & Revnivtsev 2000). In the subsequent publication (Revnivtsev et al. 2000, in preparation) we perform similar analysis for the accreting neutron stars.

Acknowledgements. Authors thank Rashid Sunyaev for numerous discussions, William Zhang for helpful discussions of PCA deadtime, Alan Smale and Keith Jahoda for the useful comments on the PCA operations. This research has made use of data obtained through the High Energy Astrophysics Science Archive Research Center Online Service, provided by the NASA/Goddard Space Flight Center. M.Revnivtsev acknowledges partial support by RFBR grant 00-15-96649.

References

- Balbus S., Papaloizou J. 1999, ApJ 521, 650
 Barret D. 2000, in Proc. of ROSSI-2000, Greenbelt, USA, p.E136
 Belloni T., Hasinger G. 1990, A&A 227, L36
 Bradt H., Rothschild R., Swank J. 1993, Astron. Astrophys. Suppl. Ser. 97, 355
 Cui W., Heindl W. A., Rothschild R. E. et al. 1997, ApJ 474, 57L
 Giles A. B. 1981, MNRAS 195, 721
 Giles A. B. 1995, PCA Housekeeping (Sec.15) <http://lheawww.gsfc.nasa.gov/docs/xray/xte/pca/document.html>
 Giles A.B., Jahoda K., Strohmayer T. 1998, Adv.Sp.Res. 22, 965
 Jahoda K., Swank J., Giles A., Stark M., Strohmayer T., Zhang W., 1996, in Proc. SPIE 2808, 59
 Jahoda K., Stark M., Strohmayer T., Zhang W., Morgan E., Fox D., 1997, in Proc. of the Symposium “The Active X-ray Sky”, astro-ph/9712340
 Jahoda K. 1998, http://lheawww.gsfc.nasa.gov/users/keith/inst_timing/index.html
 Jahoda K. 2000, <http://lheawww.gsfc.nasa.gov/users/keith/pca.ps>
 Jernigan J.G., Klein R., Arons J., 2000, ApJ, 530, 875
 Meekins J., Wood K., Headler R. et al. 1984, ApJ 278, 288
 Miyamoto S., Kitamoto S. 1989, Nat. 343, 773
 Miyamoto S., Kimura K., Kitamoto S., Dotani T., Ebisawa K., 1991, ApJ, 383, 784
 Nowak M., Vaughan B. 1996, MNRAS 280, 227
 Nowak M., Vaughan B., Wilms J. et al. 1999, ApJ 510, 874
 Payne D. 1980, ApJ, 237, 951
 Pozdnyakov L., Sobol I. & Sunyaev R. 1983, SSRvE 2, 189
 Rothschild R., Boldt E., Holt S. et al. 1974, ApJ 189, L13
 Sunyaev R. 1972, Soviet Astron.J., 49, 1153
 Sunyaev R., Titarchuk L. 1980, A&A 86, 121
 Sunyaev R., Revnivtsev M. 2000, A&A accepted, astro-ph/0003308
 Vikhlinin A., Churazov E., Gilfanov M., 1994, A&A, 287, 73
 Wen H., Bloom G., Scargle J. et al. 1996, AAS HEAD Meeting, San Diego
 Zhang W., Jahoda K., Swank J., Morgan E., Giles A., 1995, ApJ, 449, 930
 Zhang W., Morgan E., Jahoda K., Swank J., Strohmayer T., Jernigan G., Klein R., 1996, ApJ Letters, 469, 29